Available online at www.sciencedirect.com
SCIENCE DIRECT®
Journal of Power Sources 143 (2005) 150–157
JOURNAL OF POWER SOURCES
www.elsevier.com/locate/jpowsour

Diagnostic tools for liquid water in PEM fuel cells☆

Jürgen Stumper*, Michael Löhr, Stephen Hamada

Ballard Power Systems, 4343 North Fraser Way, Burnaby, BC, Canada V5J 5J9

Received 29 October 2004; accepted 26 November 2004
Available online 19 January 2005

Abstract

This paper describes a novel diagnostic test method that provides insight into the distribution of liquid water in a fuel cell under operation. The amount and distribution of liquid water in a fuel cell is measured indirectly through the measurement of certain physico-chemical properties which are functions of the liquid water content.

The MEA resistance and electrode diffusivity (MRED) method allows the measurement of (i) the pure ohmic cell resistance, (ii) the effective diffusivity of the electrodes and (iii) the free gas volume of the fuel cell. The pure ohmic resistance enables the determination of the membrane water content whereas the free gas volume measurement allows the amount of liquid water in both the anode and cathode compartments to be deduced. The MRED method was used to study the pure ohmic resistance distribution during a drying/re-hydration cycle and the effective oxygen diffusion coefficient of the cathode electrode. Furthermore, the accuracy of the liquid water volume determination was investigated.

Keywords: Fuel cells; Diagnostic tools; Water management

1. Introduction

One of the main obstacles impacting fuel cell development progress is the fact that many of the fundamental processes still are only partially understood. Consequently, fuel cell development has been relying heavily on empirical evaluation through testing which is both time consuming and expensive. In order to increase the benefit of fuel cell testing it is necessary to maximize the amount of information that can be extracted by utilizing advanced diagnostic methods and procedures. Such information can then be used (i) to support development of empirical correlations and/or (ii) to validate theoretical models predicting cell performance as function of operating conditions and characteristic properties.

Liquid water plays a key role in PEM fuel cells because its presence is closely linked to the functionality of the main components of the *unit cell* (Fig. 1). For example, the ionic conductivity of the most commonly used perfluorosulfonic acid (PFSA) electrolyte membrane Nafion® increases almost linearly with water content. Therefore, the water content of the membrane should be larger than a threshold value (minimum condition) under all operating conditions. The gas diffusion electrode (GDE) can be divided into the gas diffusion layer (GDL) and the catalyst layer (CAL). The catalyst layer mainly consists of catalyst particles, ionomer and pore space each of which are critical for the formation of the three-phase boundary where the electrochemical reactions take place. If the CAL contains too little water, its ionic conductivity will drop and not all of the catalyst surface will be accessible, which will contribute to resistive and kinetic cell voltage losses. Too much liquid water on the other hand will impede reactant gas transport and lead to mass transport related performance losses. Similarly, liquid water in the GDL will impede gas transport from the flow channels to the catalyst layer. Consequently, the water content of the catalyst layer should lie between a minimum and a maximum value (optimum condition) and the GDL water content should be less than a maximum value (maximum condition). Finally, the amount of liquid water in the channels should also obey a

☆ This paper was presented at the 2001 Fuel Cell Seminar in San Antonio, TX, USA.

* Corresponding author. Tel.: +1 604 454 0900; fax: +1 604 412 4700.
E-mail address: jurgen.stumper@ballard.com (J. Stumper).

0378-7753/$ – see front matter © 2004 Elsevier B.V. All rights reserved.
doi:10.1016/j.jpowsour.2004.11.036

Nomenclature

List of symbols

A	cell active area (m^2)
$b = 2.303\Re T/\alpha nF$	Tafel slope (V)
c	oxygen concentration (mol m^{-3})
$c_{cat}(t)$	oxygen concentration at the catalyst layer (mol m^{-3})
$c_{ch}(t)$	oxygen concentration in the channel (mol m^{-3})
c_{H^+}	proton activity at the catalyst (mol m^{-3})
c_{H_2O}	water activity at the catalyst (mol m^{-3})
$c_0 = c_{ch}(0)$	initial oxygen concentration (mol m^{-3})
D_{eff}	effective O_2 diffusion coefficient (m^2 s^{-1})
$E_{cell}(t)$	cell voltage (V)
$E_{cell}(0)$	initial cell voltage (V)
$E_c^0(t)$	reversible cathode potential (V)
$E_{cell}^0(t)$	reversible cell voltage (V)
F	Faraday's constant (9.648×10^4 C mol^{-1})
i	current density (A m^{-2})
$i_{max} = 4FD_{eff}c_{ch}/L$	limiting current density (A m^{-2})
i_0	exchange current density (A m^{-2})
I	current (A)
L	thickness of the GDL (m)
n	number of electrons transferred
n_{mol}	number of moles
p	gas pressure (Pa)
R	cell resistance (Ω m^2)
$\Re$	ideal gas constant (8.314 J K^{-1} mol^{-1})
T	temperature (K)
V	free gas volume (m^3)
z	coordinate perpendicular to MEA (m)

Greek letters

$\eta(t)$	activation over-potential (V)
$\eta_{mt}(t)$	mass transport over-potential (V)

Subscripts

a	anode
c	cathode

maximum condition as the presence of liquid water in the flow channels increases gas flow resistance, which in turn increases the parasitic load of supplying the reactant gases.

Because water management is critical for durability and performance of PEM fuel cells, Ballard has been developing advanced diagnostic tools to study the distribution and movement of water within the unit cell. Among the requirements for such diagnostic tools are (i) in situ applicability, (ii) minimal invasiveness and (iii) ability to provide local information, i.e. information on the distribution of liquid water over the active area. To date, there is only one diagnostic method known to the authors that fulfills all three of the above requirements: neutron-imaging [1]. However, the necessary

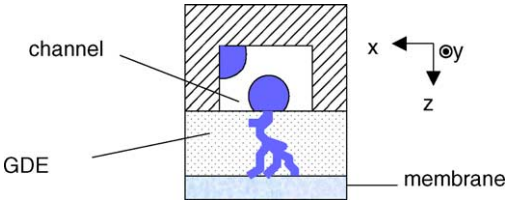

Fig. 1. Schematic cross section of a PEM fuel cell indicating the possible presence of liquid water in membrane, GDE and channel.

neutron sources are available only at few research institutes worldwide equipped to deal with radioactive radiation.

Consequently, we have taken an alternative approach which relies on (i) the measurement of characteristic fuel cell properties and (ii) the back-calculation of the water content from the known dependence of these properties on water content. For example, the water content of the membrane can be determined from the membrane ohmic resistance using the known relationship between proton conductivity and water content [2]. The membrane ohmic resistance can be determined from the ohmic resistance of a fuel cell if the contributions of the other cell components such as electrodes and plates are known. Recently, a novel method for the determination of the pure ohmic resistance of a fuel cell was presented using the membrane resistance and electrode diffusivity (MRED) [3] method. In this paper we show that through a combination of the MRED method with current mapping [4,5] it is possible to obtain further information on the local membrane water content distribution across the cell area. To this end the MRED method is performed using a custom designed cell hardware with segmented current collection plates allowing measurement of the current distribution along the length of the unit cell. Using the MRED method, profiles of the mass-transport free membrane resistance can be obtained. In addition, the cell hardware allows the investigation of dynamic phenomena such as transient drying and re-hydration of the membrane by monitoring changes in current distribution over time. Such investigations are particularly interesting for automotive applications, which are characterized by dynamic load cycles with high turn-down ratios leading to non-stationary operation over significant time periods. The characterization of the water distribution in the cell under such non-stationary conditions is of crucial importance for the improvement of fuel cell reliability and durability.

2. Experimental

The experimental results were obtained using a single Ballard^{TM} Mk 9 fuel cell. The test cell was operated with a current collection plate segmented on the cathode along the reactant flow direction (see Fig. 2); the flowfield plate and gas diffusion layers were not segmented allowing the use of standard flowfield plates and membrane electrode assemblies (MEAs). In order to correct for in-plane currents in the

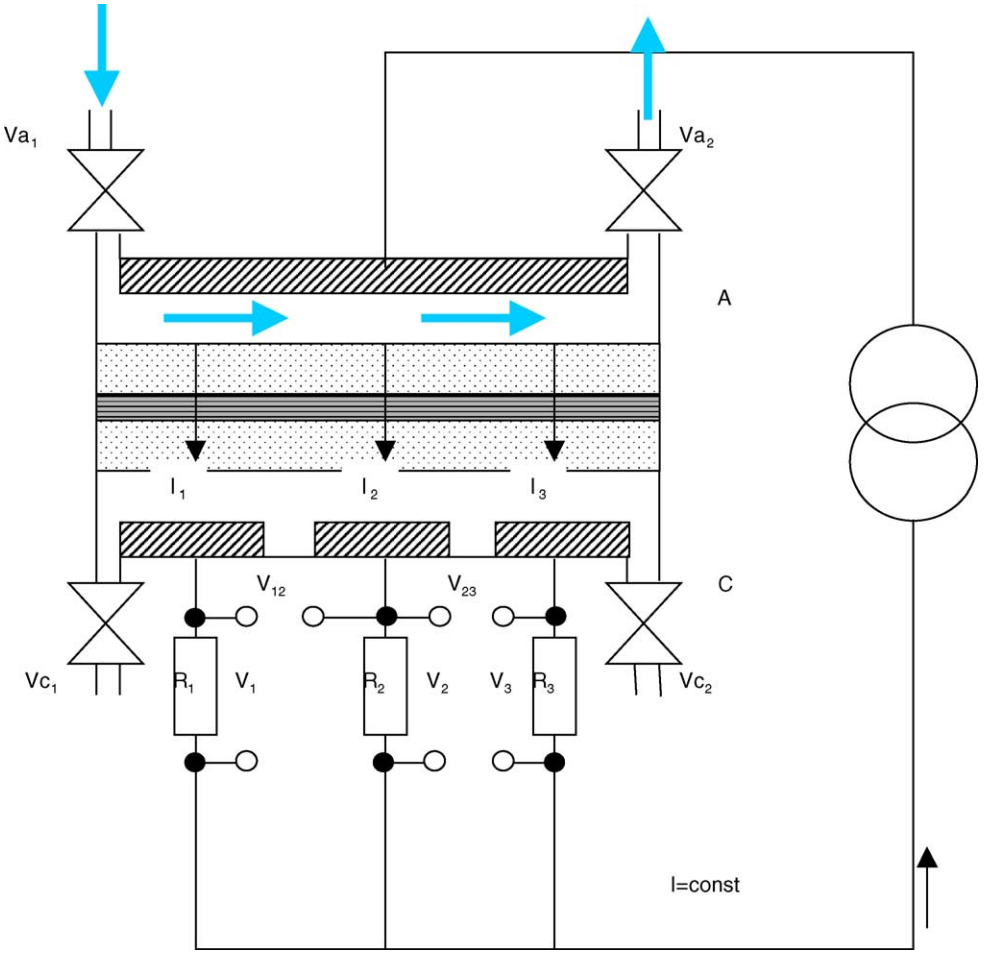

Fig. 2. Schematic diagram of the experimental setup for a cell voltage decay experiment in combination with current mapping. R_i: shunt resistors, V_i: shunt voltages, V_{ij}: in-plane voltages. Operating conditions: H_2/O_2, H_2 stoichiometry 1.5, cathode inlet (V_{c_1}) and outlet (V_{c_2}) valves closed, arrows on anode side indicate gas flow during cathode discharge. Only three shunt resistors are shown for simplicity.

flowfield plate, both the voltages V_i across the shunt resistors R_i as well as the in-plane voltages $V_{i,i+1}$ were measured (where $i = 1, \ldots, 16$). This allowed the determination of the true through plane currents I_i through the MEA.

For a transient polarization, the cell was first run under prescribed operating conditions until a steady state was reached. Then current flow was interrupted and the cell was switched to O_2 as oxidant until the cathode compartment was completely filled with O_2 and the pressure the same as on the anode side. Thereafter the inlet and outlet valves on the cathode side were closed and the cell was discharged at constant current while the H_2 flow was kept constant. During the discharge, the currents through the shunt resistors, in-plane currents and cell voltages were recorded. Then the oxidant inlet valve was opened, the cathode compartment refilled with O_2 and the cell discharge was repeated at the next current. Typically, transient polarizations were recorded starting with the highest current in descending order. In order to minimize any change in membrane hydration due to product water which might affect the resistance distribution, the duration of the discharge was limited to about 100 C (partial discharge) for each current point of a transient polarization.

For a cathode diffusivity determination, the cell discharge was continued until the current through the external load decayed to zero (complete discharge) corresponding to a charge of about 1500 C. In addition to the currents and voltages, the pressure on the cathode side was also recorded during the discharge.

For the determination of the amount of liquid water, a complete discharge was performed with H_2/O_2 as reactants and inlets as well as outlet valves closed on both the anode and cathode side. In addition to the currents and voltages, the gas pressures on the anode and cathode side were also recorded during the discharge. Cell temperatures are given by the coolant inlet temperature.

3. Results and discussion

3.1. Determination of the pure ohmic resistance of a fuel cell

The cell voltage of a fuel cell under current flow is determined by a number of loss mechanisms that are kinetic,

resistive or mass transport related. Mass transport losses are a major cause for performance inefficiencies especially on the cathode. One method to determine the ohmic voltage losses as function of current density is a fit of Eq. (1) to the steady state polarization curve. However, this approach suffers from an interdependence of the ohmic and mass transport related parameters R, i_{max} in the equation so that often no unique solution is found.

$$E = E^0_{cell} - b\log\left(\frac{i}{i_0}\right) - b\log\left(\frac{i_{max}}{i_{max} - i}\right) - iRA \qquad (1)$$

One way to circumvent this problem is to determine the ohmic cell resistance through AC-impedance spectroscopy [6]; however, the corresponding experimental setup is more complex requiring specialized equipment such as lock-in amplifiers or frequency response analyzers particularly if spatial resolution is desired [7]. The MRED method works in the time – instead of the frequency domain and utilizes a galvanostatic cell-discharge with interrupted reactant supply. For an experiment on the cathode, the reactant flow is stopped by closing the inlet and outlet valves on the cathode side, the cell current is switched on and the voltage–time transient is recorded. As there is no gas flow, reactant concentration gradients along the flow channels are eliminated. After the current has been switched on, the O_2 concentrations in the channel and at the catalyst layer become time dependent, leading to a time dependent mass transport over-potential $\eta_{mt}(t)$.

$$\eta_{mt}(t) = b\log\left(\frac{i_{max}}{i_{max} - i}\right) = b\log\left(\frac{c_{ch}(t)}{c_{cat}(t)}\right) \qquad (2)$$

At $t = 0$ however, the mass transport over-potential is zero because $c_{ch}(0) = c_{cat}(0) = c_0$. Consequently, the mass transport over-potential rises from zero on a timescale determined by the relaxation time t_r of the reactant transport from the channel to the catalyst layer. Assuming that this transport process is of diffusive nature and can be described by an effective diffusion coefficient D_{eff}, then $t_r = L^2/D_{eff}$. If the initial cell voltage $E_{cell}(0)$ is measured on a timescale smaller than t_r, i.e. *before* concentration gradients across the GDL have developed, then the cell voltage measurement is mass transport free. With $L = 0.025$ cm and $D_{eff} \approx 6 \times 10^{-3}$ cm^2 s^{-1} we get $t_r \approx 0.1$ s.

Repeating the measurement of $E_{cell}(0)$ for different currents i yields the transient polarization $E_{cell}(0,i)$ which is free of mass transport contributions and contains only ohmic and kinetic losses [3]. Fig. 3 shows the cell voltage transients for complete galvanostatic discharges at different current densities against charge, therefore all transients have the same duration of about 1500 C, which is a function of the amount of O_2 in the cathode volume and the current/voltage characteristic of the electronic load.

From the previous discussion it follows that the pure ohmic resistance of the fuel cell can determined by a fit of the simplified Srinivasan equation (3) [8] to the experimental data.

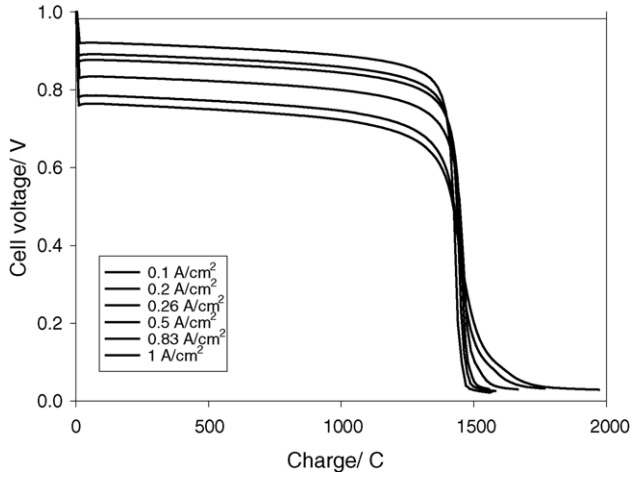

Fig. 3. Transients of the average cell voltage for various average current densities plotted against charge. Operating conditions: H_2/O_2, $T = 75\,^\circ$C, $p = 45$ psia, fuel inlet open, fuel outlet closed, oxidant inlet and outlet valves closed. The topmost curve of the graph corresponds to the lowest current density. The initial cell voltage $E_{cell}(0)$ is measured for times $t < 0.1$ s.

$$E = E^0_{cell} - b\log\left(\frac{i}{i_0}\right) - iRA \qquad (3)$$

3.2. Membrane water content

For Nafion® membranes, the proton conductivity is a strong function of the water content. If the membrane resistance and membrane thickness are known, the membrane water content can be deduced using literature data [2]. The membrane ohmic resistance can be calculated from the cell resistance by subtracting the bulk resistances of the flowfield plates and electrodes as well as the contact resistances from the pure ohmic cell resistance determined with the transient polarization. By combining the cell voltage decay experiment with current mapping, spatially resolved transient polarizations corresponding to each of the collector plate segments can be obtained. Fig. 4 shows a series of 16 transient polarization curves and the corresponding pure ohmic resistance distribution of the fuel cell determined from a fit of Eq. (3). The latter shows a characteristic "bathtub" shape, indicating membrane drying at the inlets of both reactants. This type of membrane hydration profile is typical under operation with sub-saturated gases.

Fig. 5 shows a drying and re-hydration experiment where the humidification was switched off (a) and then on again (b) and the resulting shift in current distribution was monitored over time. The individual currents are numbered from the oxidant inlet (1) to the oxidant outlet (16) and it can be seen that drying occurs at the oxidant inlet with the highest rate. Also, whereas the current at the oxidant inlet drops quickly to about 50% of its previous value, the current further down the channel actually increases (see currents # 8, 16). This current shift towards the oxidant outlet is a consequence of

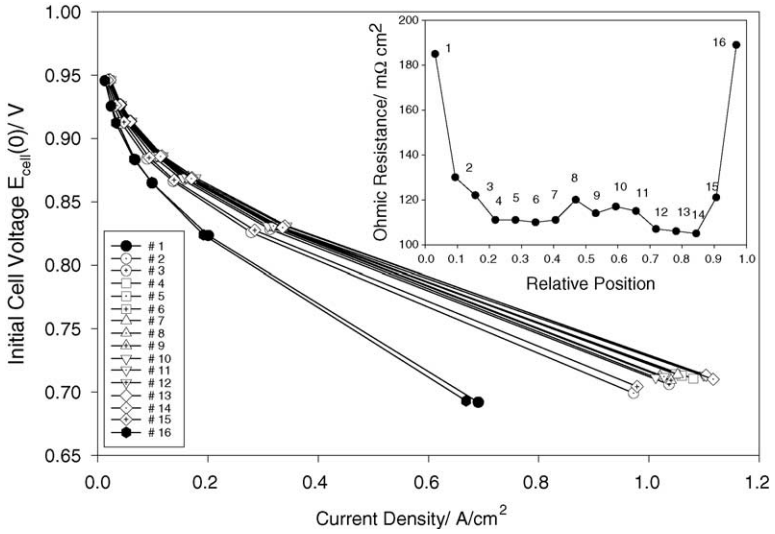

Fig. 4. Transient polarization curves for operation on H_2/O_2. Numbers denote the individual current collector elements along flow channel length (y-direction). Inset: the resulting pure ohmic resistance distribution $R(y)$ as determined from a fit of Eq. (2). Oxidant inlet: left, fuel inlet: right (counterflow operation). Operating conditions before transient polarization: $i = 1$ A cm^{-2}, H_2/air stoichiometry 1.6/1.8, $T = 65\,^{\circ}$C, $p = 45$ psia, RH = 50% for both H_2, air.

the higher gas flow on the oxidant side resulting in a higher drying power and the fact that the total current remains constant during the experiment. In order to determine the effect of the dry operation on the resistance distribution, a transient polarization was performed after the 20 min of dry operation in Fig. 5a and the results are shown in Fig. 6 together with the baseline resistance distribution corresponding to operation with fully humidified gases. Again, the typical bathtub shape is visible, but in contrast to Fig. 4, the resistance at the oxidant inlet is now much higher relative to the middle of the cell (350 mΩ cm^2 compared to 150 mΩ cm^2). This ohmic resistance profile is in accordance with the observed current shift away from the oxidant inlet towards the oxidant outlet.

The comparison of Fig. 5a and b also shows that upon switch-back to humidified gases the recovery of cell voltages and currents occurs significantly faster than their decay during drying. Whereas the cell voltages show a gradual, almost linear decrease during drying, they recover almost instantaneously after switch-back to humidification. This appears to be true also for the partial currents, all of them showing a much faster change in the first ≈75% of their total recovery. I_1 at the oxidant inlet appears to have the slowest recovery compared to the other partial currents; this may be due

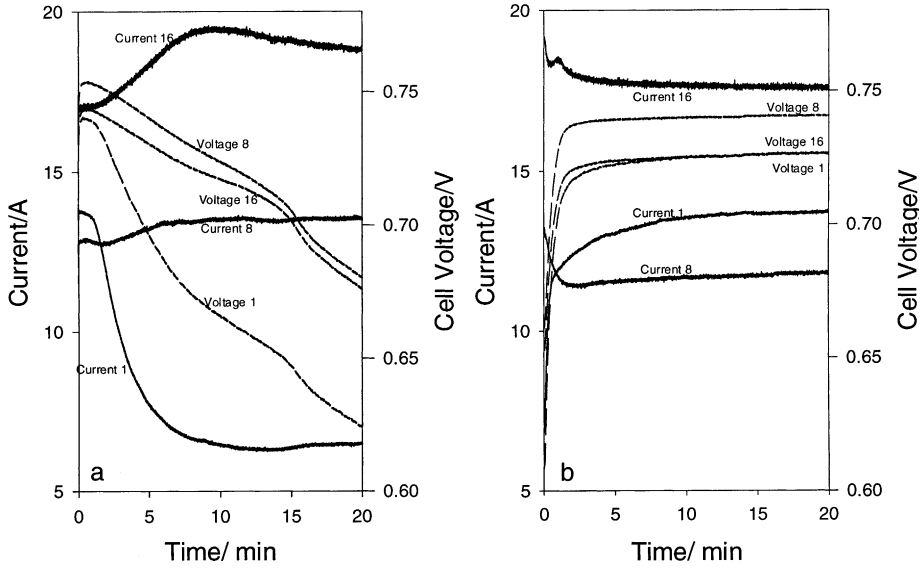

Fig. 5. Local currents (solid lines) and cell voltages (dashed lines) (a) after switching from RH = 100% to dry reactant gases and (b) after switch-back to RH = 100%. For clarity only the currents at oxidant inlet (1), middle (8) and fuel inlet (16) are shown. Operating conditions H_2/O_2, H_2/O_2 stoichiometry 1.6/8.0, $I_{tot} = 260$ A, counterflow operation, $T = 70\,^{\circ}$C, $p = 45$ psia.

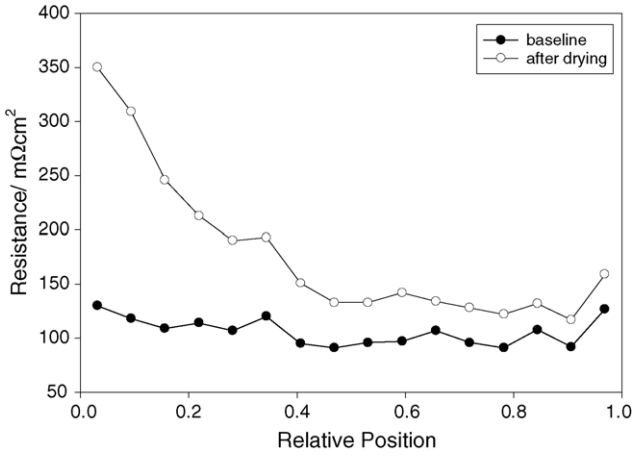

Fig. 6. Pure ohmic resistance profile after 20 min operation without humidification (open circles, see also Fig. 5a) compared to a baseline profile for operation with fully humidified gases (full circles). Operating conditions as in Fig. 5.

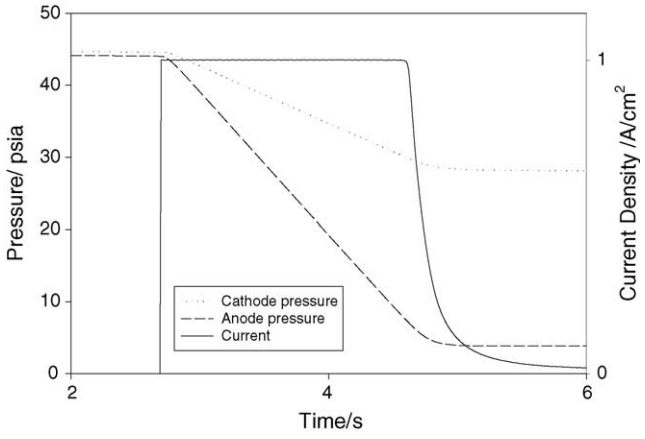

Fig. 7. Pressure decay during a galvanostatic cell discharge at 1 A cm^{-2}. Conditions: $p = 45$ psia, $T = 70\,^{\circ}$C, H_2/O_2 operation, fuel/ox inlet and outlet valves closed. Solid line: current, dashed lines: anode and cathode pressure.

to the fact that membrane re-hydration is also a function of water production, which is lowest at the oxidant inlet. The difference in drying and re-hydration rates can have important implications for the dynamic operation of fuel cells in automotive applications. The control of membrane hydration is also of critical importance for rapid startup from ambient and sub-zero temperatures.

3.3. Free cell volume

In addition to the pure ohmic resistance, the experimental setup allows the determination of the free gas volume of the unit cell (between the inlet and outlet valves). If the free gas volume is known for the dry state of the fuel cell (V_{dry}), the volume of liquid water present under a given operating condition on the anode or cathode can simply be determined by subtracting the corresponding free gas volume V_{wet}.

During the galvanostatic discharge, the inlet and outlet valves are closed and consequently reactant gas is consumed at the constant rate of

$$\frac{\mathrm{d}}{\mathrm{d}t} n_{\mathrm{mol}} = \frac{I}{nF} \tag{4}$$

where n_{mol} is the number of moles, I the current, $n = 2$ or 4 for H_2 or O_2, respectively, and F Faraday's constant. On the other hand, using the ideal gas law

$$\frac{\mathrm{d}}{\mathrm{d}t} n_{\mathrm{mol}} = \frac{V}{\Re T} \frac{\mathrm{d}}{\mathrm{d}t} p \tag{5}$$

where p, V, T denote pressure, volume and temperature, respectively, and $\Re$ the gas constant. Using Eq. (4) and (5) it follows:

$$V = \frac{\Re T}{\mathrm{d}p/\mathrm{d}t} \frac{I}{nF} = \frac{1}{\mathrm{d}c/\mathrm{d}t} \frac{I}{nF} \tag{6}$$

where c denotes the reactant concentration. Eq. (6) allows the determination of the gas filled (free) volume on the anode or cathode side from the pressure change during a galvanostatic cell discharge. If the valves on both anode and cathode side are closed, the free gas volumes on both sides can be determined simultaneously. Fig. 7 shows the result of such an experiment and it can be seen that the H_2 pressure drops about twice as fast as the O_2 pressure as expected if the gas free volumes are about the same on both the anode and cathode side.

The first derivatives of the pressure versus time curves typically show a distinctive plateau which can be used for the volume determination with Eq. (6). In order to minimize effects due to external leaks or gas permeation through the membrane it was found to be advantageous to perform the discharge at current densities >0.5 A cm^{-2}.

In order to verify the accuracy of the free volume determination, known amounts of water were added to the fuel cell through faradaic production and the corresponding change in volume V_{wet} was measured. During water addition, both the fuel and oxidant outlet valves were closed in order to make sure that all product water remained inside of the cell. With this arrangement, the cell was run for about 10 000 C on H_2/O_2 corresponding to a water production of ≈0.9 ml and the volume was determined with a galvanostatic discharge. This cycle was repeated several times and the free anode and cathode volumes were plotted against the product water produced.

The results in Fig. 8 demonstrate the accuracy of determination of the *total* amount of liquid water (anode + cathode) in the cell with an error of $\varepsilon = 4 \times 10^{-3}$. On the other hand, the slope for the cathode shows a large deviation from 1 and the anode slope even a negative value. This indicates that a significant amount of water is dragged from the anode to that cathode during faradaic water production between consecutive volume determinations. The slope of the anode line gives directly the water transfer factor

$$\alpha = \frac{\mathrm{H_2O\,(transferred\ from\ } A \rightarrow C)}{\mathrm{H_2O\,(produced)}} \tag{7}$$

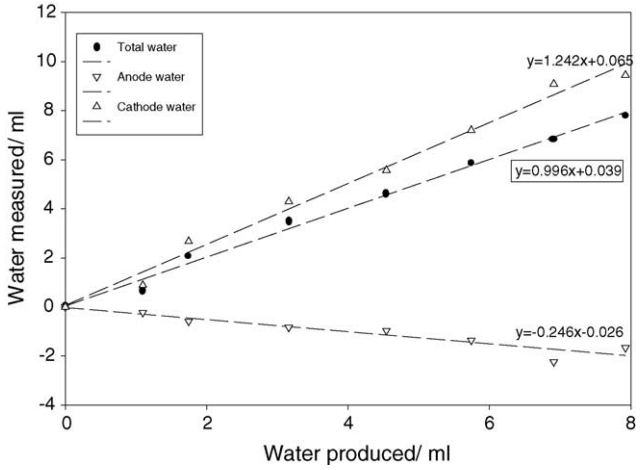

Fig. 8. Calibration of the volume determination method conducted at $1\,A\,cm^{-2}$ using product water and H_2/O_2 as reactants. The small deviation from unity of 4×10^{-3} for the slope of the total (=anode + cathode) water demonstrates the accuracy of the volume determination. The negative slope for the anode water gives the transfer factor from anode to cathode.

and from Fig. 8 we conclude $\alpha = 0.246$ for these particular operating conditions. This indicates water transport in the same direction but at a slightly larger value than the range $-0.05 < \alpha < 0.2$ which was observed previously for operation with H_2/air and gas flow on both anode and cathode side [9].

3.4. Cathode diffusivity

On the cathode side, mass transport losses associated with transport of reactants and products to and from the active catalyst sites are a major cause of inefficiencies in fuel cells. A large part of these mass transport losses is associated with diffusion/convection processes through the porous electrode structure. A technique for the determination of these diffusion losses under operating conditions would therefore be of great value for the improvement of fuel cell performance. In this section it will be discussed how the galvanostatic cathode discharge of a fuel cell allows the determination of the cathode diffusivity.

After the initial relaxation processes have subsided, i.e. for for $t \gg t_r$ the fuel cell exhibits quasi-stationary behavior during a galvanostatic discharge and the current i can be written using Fick's law

$$D_{\text{eff}} \frac{\partial c}{\partial z} = \frac{i}{4F} \tag{8}$$

or, assuming a linear concentration gradient across the GDL:

$$\Delta c = c_{\text{ch}}(t) - c_{\text{cat}}(t) = \frac{iL}{4FD_{\text{eff}}} \tag{9}$$

where $c_{\text{cat}}(t)$ denotes the oxygen concentration at the catalyst, $c_{\text{ch}}(t)$ the oxygen concentration in the flow channels, L the GDL-thickness, D_{eff} the effective diffusivity of the GDL and F Faraday's constant. Although $c_{\text{cat}}(t)$, $c_{\text{ch}}(t)$ are functions of time, Eq. (9) implies that the difference in concentrations between flow channel and catalyst is constant during the galvanostatic transient if this is also true for D_{eff}. Consequently, if both $c_{\text{cat}}(t)$, $c_{\text{ch}}(t)$ can be measured, the effective diffusivity can be determined. The channel concentration $c_{\text{ch}}(t)$ can be measured using a fast pressure sensor whereas the concentration at the catalyst can be calculated from the cell voltage decay $E_{\text{cell}}(t)$ as explained in the following section.

For convenience, the cell voltage decay can be expressed relative to the initial cell voltage $E_{\text{cell}}(0)$ as follows:

$$\begin{aligned}\Delta E_{\text{cell}}(t) &= E_{\text{cell}}(0) - E_{\text{cell}}(t) \\ &= E^0_{\text{cell}}(0) - \eta_c(0) - E^0_{\text{cell}}(t) + \eta_c(t)\end{aligned} \tag{10}$$

where E^0_{cell} is the reversible cell voltage and η_c the activation over-potential at the cathode. It is worth noting that $\Delta E_{\text{cell}}(t)$ contains no ohmic losses, as they are constant during discharge. Due to the continuous supply of H_2, we also assume no change in the activation over-potential at the anode.

The time dependence of E^0_{cell} can be calculated using Nernst's equation for the cathode

$$E^0_c(t) = E^0_{c,\text{ref}} + \frac{\Re T}{2F} \ln\left(\sqrt{\frac{c_{\text{ch}}(t)}{c^{\text{ref}}}}\left(\frac{c_{H^+}}{c^{\text{ref}}_{H^+}}\right)^2 \frac{c^{\text{ref}}_{H_2O}}{c_{H_2O}}\right) \tag{11}$$

where $E^0_c(t)$ denotes the reversible cathode potential. $E^0_c(t)$ is time dependent as the O_2 concentration $c_{\text{ch}}(t)$ in the flow channels continually decreases during the discharge. Assuming c_{H^+}, c_{H_2O} are time independent it follows:

$$E^0_{\text{cell}}(0) - E^0_{\text{cell}}(t) = \frac{\Re T}{2F} \ln\left(\sqrt{\frac{c_{\text{ch}}(0)}{c_{\text{ch}}(t)}}\right) \tag{12}$$

$\eta_c(t)$ can be expressed as function of the oxygen concentration at the catalyst layer using the Tafel equation

$$i(t) = i_{0c} \frac{c_{\text{cat}}(t)}{c_{\text{ref}}} \exp\left(2.303 \frac{\eta_c(t)}{b_c}\right) \tag{13}$$

where i_{0c} denotes the exchange current density, c_{ref} a reference concentration (e.g. $p_{O_2} = 1$ atm) and b_c the Tafel slope which leads to

$$\eta_c(t) - \eta_c(0) = b_c \log\left(\frac{c_{\text{cat}}(0)}{c_{\text{cat}}(t)}\right) \tag{14}$$

With (12) and (14) Eq. (10) simplifies to

$$E_{\text{cell}}(0) - E_{\text{cell}}(t) = b_c \log\left(\frac{c_{\text{cat}}(0)}{c_{\text{cat}}(t)}\right) + \frac{\Re T}{2F} \ln\left(\sqrt{\frac{c_{\text{ch}}(0)}{c_{\text{ch}}(t)}}\right) \tag{15}$$

Eq. (15) shows that the change in cell voltage over time is due to the change of the ratio $c_{\text{cat}}(0)/c_{\text{cat}}(t)$ at the catalyst sites corrected with respect to the change in oxygen concentration in the flowfield channels.

With (15) we can now calculate the O_2 concentration $c_{\text{cat}}(t)$ at the catalyst sites as a function of time using the fact

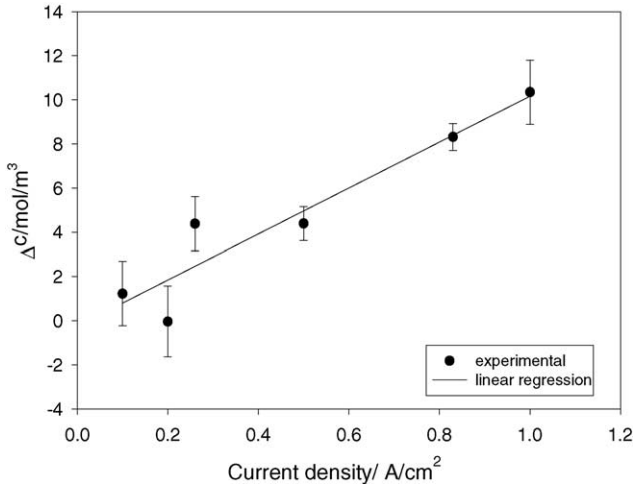

Fig. 9. Experimental plot of Δc against current density i. Circles: experimental values, solid line: straight line least-squares fit, other parameters: $b_c = 55$ mV, $T = 75\,^{\circ}$C, $L = 250\,\mu$m. Error bars represent experimental errors in voltage and pressure measurements. Experimental value for the effective O_2 diffusion coefficient: $D_{eff} = 6.1 \times 10^{-7}\,m^2\,s^{-1}$.

that without current ($t \leq 0$) the O_2 concentration at the catalyst sites equals the O_2 concentration in the flow channels. With

$$c_{cat}(0) = c_{ch}(0) = c_0 \tag{16}$$

it follows that

$$c_{cat}(t) = c_0 \exp(-(2.303/b_c) \times E_{cell}(0) - E_{cell}(t) - (\Re T/2F) \times \ln(\sqrt{c_0/c_{ch}(t)})) \tag{17}$$

In order to validate this analysis the series of galvanostatic discharge experiments shown in Fig. 3 was analyzed and Δc plotted against current density. According to Eq. (9) a plot of Δc against i should yield a straight line allowing the determination of D_{eff}. As can be seen in Fig. 9, the experimental points are very close to the expected straight line through the origin. Between each of the experiments, the fuel cell was reconditioned for about 10 min before the next discharge was performed. The slope of the straight line yields $D_{eff} = 6.1 \times 10^{-7}\,m^{-2}\,s^{-1}$. The corresponding value for the mass transfer coefficient of $D_{eff}/L = 2.44 \times 10^{-3}\,m\,s^{-1}$ is close to the value of $D_{eff}/L = 2.8 \times 10^{-3}\,m\,s^{-1}$ that was determined independently using a non-linear four-parameter-fit to experimental helox and air polarization curves obtained with a similar setup and fuel cell [9].

4. Conclusions

The galvanostatic discharge of a fuel cell (MRED method) provides important information related to the amount and distribution of liquid water in a fuel cell in a minimally invasive manner and under in situ conditions. The mass transport free transient polarization allows the determination of the pure ohmic cell resistance from which the membrane water content can be deduced. The combination of galvanostatic discharge with current mapping allows the determination of the distribution of water in the membrane across the active area. Secondly, the total free gas volume allows the determination of the total amount of liquid water present in the anode or cathode compartment. Thirdly, the cathode effective diffusivity can be determined from the pressure and voltage decay during the cell discharge. Literature data suggest that the electrode diffusivity decreases as a function of electrode water content, which might enable differentiation between water in the electrode and the flowfield channels.

References

[1] R. Satija, D.L. Jacobson, M. Arif, S.A. Werner, J. Power Sources 129 (2004) 238.
[2] K.D. Kreuer, in: W. Vielstich, A. Lamm, H. Gasteiger (Eds.), Handbook of Fuel Cells – Fundamentals, Technology Applications, vol. 3, Wiley, Chichester, UK, 2003, pp. 420–435.
[3] J. Stumper, H. Haas, A. Granados, J. Electrochem Soc., in press.
[4] A. Hakenjos, K. Tueber, J.O. Schumacher, C. Hebling, Fuel Cells 4 (2004) 185.
[5] J. Stumper, S.A. Campbell, D.P. Wilkinson, M.C. Johnson, M. Davis, Electrochim. Acta 43 (1998) 3773.
[6] B. Andreaus, A.J. McEvoy, G.G. Scherer, Electrochim. Acta 47 (2002) 2223.
[7] G. Bender, M.S. Wilson, T.A. Zawodzinski, J. Power Sources 123 (2003) 163.
[8] S. Srinivasan, E.A. Ticianelli, C.R. Derouin, A. Redondo, J. Power Sources 22 (1988) 359–375.
[9] P. Berg, K. Promislow, J. St-Pierre, J. Stumper, B. Wetton, J. Electrochem. Soc. 151 (2004) A341.